

# Multiple Critical Velocities in Oscillatory Flow of Superfluid $^4\text{He}$ due to Quartz Tuning Forks

D. Schmoranzer,<sup>1</sup> M. J. Jackson,<sup>1</sup> V. Tsepelin,<sup>2</sup> M. Poole,<sup>2</sup> A. J. Woods,<sup>3</sup> M. Človečko,<sup>4</sup> and L. Skrbek<sup>1</sup>

<sup>1</sup>*Faculty of Mathematics and Physics, Charles University,  
Ke Karlovu 3, 121 16, Prague 2, Czech Republic*

<sup>2</sup>*Physics Department, Lancaster University, Lancaster, LA1 4YB, United Kingdom*

<sup>3</sup>*National High Magnetic Field Laboratory, 1843 Stadium Rd, Gainesville, FL 32611, USA*

<sup>4</sup>*Institute of Experimental Physics, Slovak Academy of Sciences, Watsonova 47, 040 01 Košice, Slovak Republic*

We report recent investigations into the transition to turbulence in superfluid  $^4\text{He}$ , realized experimentally by measuring the drag forces acting on two custom-made quartz tuning forks with fundamental resonances at 6.5 kHz and 55.5 kHz, in the temperature range 10 mK to 2.17 K. In pure superfluid in the zero temperature limit, three distinct critical velocities were observed with both tuning forks. We discuss the significance of all critical velocities and associate the third critical velocity reported here for the first time with the development of large vortical structures in the flow, which thus starts to mimic turbulence in classical fluids. The interpretation of our results is directly linked to previous experimental work with oscillators such as tuning forks, grids and vibrating wires, focusing on the behavior of purely superfluid  $^4\text{He}$  at very low temperatures.

PACS numbers: 67.25.dk, 67.25.dg, 77.65.Fs, 47.27.Cn

## I. INTRODUCTION

To this day, turbulent motion of fluids remains the last unresolved problem of classical physics and presents many practical challenges across many different areas of industry. In contrast to its classical counterpart, quantum turbulence may only occur in superfluids and was historically first observed in superfluid helium<sup>1</sup>. In  $^4\text{He}$  at very low temperature, quantum turbulence takes the form of a dense dynamic tangle of singly quantized vortices moving in a fluid with virtually no viscous dissipation. Compared to classical turbulence, it can be regarded as a conceptually simpler system to develop theoretical models for and to simulate numerically<sup>2</sup>, and may provide a stepping-stone to a better understanding of turbulence in general. This is supported by the mounting evidence that quantum turbulence, when probed at large length scales, shares many of the general properties of turbulence in classical viscous fluids<sup>3</sup>. Abounding evidence on the quasi-classical nature of certain quantum flows can be readily found in the literature on steady-state and decay experiments using channel flow setups in the two fluid regime<sup>4,5</sup>, on measurements of vortex tangle decay at low temperatures<sup>6,7</sup>, numerical simulations<sup>8</sup> or even Andreev reflection experiments<sup>9</sup> in  $^3\text{He}$ . It is currently understood<sup>10</sup> that these classical-like properties are related to partial polarization of quantized vortices that effectively form bigger bundles within a turbulent tangle, mimicking the appearance of large energetic eddies in classical turbulence<sup>11</sup>. Recent developments in quantum turbulence in  $^4\text{He}$  are summarized in several review articles<sup>12–16</sup>.

One of the signs of quasi-classical behaviour expected in turbulent flows due to submerged oscillators is that the drag coefficient should display a plateau at a value near unity at higher velocities (c.f. oscillating cylinder in water<sup>17,18</sup>). In analogy to classical fluid dynamics, we

define the drag coefficient as  $C_D = 2F/(A\rho v^2)$  with  $F$ ,  $A$ ,  $\rho$ , and  $v$  representing the peak force, cross-sectional area of the body perpendicular to the direction of motion, fluid density, and peak velocity, respectively. It is therefore somewhat surprising that the reported drag coefficients are typically one or even two orders of magnitude lower<sup>19–22</sup> and that no distinct cross-over between “ultra-quantum” (unpolarized) and “quasi-classical” (polarized, with larger structures) oscillatory flow has been directly observed in the zero temperature limit so far. It should, however, be noted that exceptions exist, where drag coefficient of order unity has been obtained even at millikelvin temperatures with grids<sup>23</sup> or commercial tuning forks<sup>24</sup> (the latter converted to drag coefficient in Ref. 25, Fig. 5).

It was shown that in purely superfluid  $^4\text{He}$  in the zero temperature limit (effectively a physical vacuum with ballistically propagating thermal excitations), quantum turbulence can be generated by a mechanical oscillator above some clearly defined critical velocity<sup>19,20,25,26</sup>. Usually, it is observed that the drag force acting on such an oscillator increases sharply at this critical velocity and later tends towards an approximately quadratic velocity dependence. The behavior close to the initial instability may be hysteretic<sup>19,26–28</sup>, and generally the nucleation of turbulence may appear to be history dependent<sup>29</sup>. Additionally, previous work<sup>20–22,30,31</sup> has reported the observation of two critical velocities, interpreting the lower one as an initial instability typically described as the formation of a thin layer of quantized vorticity near the oscillator, and the higher one (marking a rapid onset of extra dissipation) as the production of large amounts of quantized vorticity or as the flow developing large vortical structures similar to those in turbulent classical fluids.

On the other hand, instabilities in classical flows due to oscillating objects related to the onset of turbulence are not governed by any well-defined critical value of ve-

locity, but rather by dimensionless parameters such as the Reynolds number, the Stokes number, the Keulegan-Carpenter number<sup>17,18</sup> or by the Strouhal number in case of periodic vortex shedding by a bluff body in steady flow<sup>32</sup>. This leads to the suggestion that in superfluid helium above 1 K (in the “two-fluid regime”), several scenarios of transition to turbulence are possible, depending on whether the normal component or the superfluid component becomes unstable first, and on the degree of coupling between them<sup>16</sup>. In this case, the turbulent flow created at high velocity exhibits a drag coefficient near unity<sup>19,23–25,33</sup>, in striking contrast to the situation at low temperatures. However, for a better understanding of the situation in the two-fluid regime, it is essential to first study the limiting cases, i.e., the behavior of a fully classical fluid above the superfluid transition ( $T_\lambda = 2.178$  K), as well as that of pure superfluid in the zero temperature limit and connect them with systematic measurements throughout the entire range of temperatures.

In this manuscript, we will focus on the behaviour of isotopically pure superfluid  $^4\text{He}$  in the zero temperature limit (with higher-temperature data shown for comparison), specifically on the flow due to quartz tuning forks, and we will present convincing evidence for three distinct hydrodynamic critical velocities and suggest a tentative explanation of the related flow instabilities.

## II. EXPERIMENTAL DETAILS

Quartz tuning forks are now well-established probes of cryogenic helium flow<sup>34</sup>. They have been used to produce and detect turbulence in superfluids and usually exhibit a distinct critical velocity that can be determined from the measurement of the drag force as a function of velocity<sup>19,33</sup>. When sufficient care is taken to eliminate parasitic effects such as cavitation<sup>35,36</sup> or acoustic emission<sup>37,38</sup>, the frequency dependence of this critical velocity is consistent with the square root dependence which can be expected in both classical<sup>39</sup> and quantum<sup>40</sup> turbulence.

The experiments presented here were conducted in Prague and Lancaster independently, using quartz tuning forks produced from the same monocrystalline wafer. The Prague experimental cell (a gold-plated copper cylinder of 32 mm diameter and 172 mm height) contains – amongst other types of vibrating structures that will not be discussed here – a tuning fork resonating at 6.5 kHz. Its dimensions are given as length  $L = 3.50$  mm, tine thickness (parallel to the direction of motion<sup>34</sup>)  $T = 90$   $\mu\text{m}$  and width  $W = 75$   $\mu\text{m}$  (original wafer thickness). The distance between its two prongs is  $D = 90$   $\mu\text{m}$ . The tuning fork was enclosed in a 10 mm long open-topped stainless steel capillary of 2.4 mm inner diameter to restrict the geometry and to help suppress acoustic damping. The 6.5 kHz tuning fork was used in two different flexural resonant modes – the fundamental resonance at

6.5 kHz and the first overtone at 40.0 kHz. The gold-plated copper cell was mounted on to the mixing chamber of a Leiden Cryogenics MNK126-400  $^3\text{He}/^4\text{He}$  dilution refrigerator with a base temperature below 10 mK. The cell was filled with isotopically pure<sup>41</sup>  $^4\text{He}$  with  $^3\text{He}$  content below  $10^{-13}$  via a thin thermally-anchored stainless steel capillary. The temperature of the mixing chamber was monitored by a calibrated ruthenium oxide thermometer attached to the mixing chamber flange.

Another tuning fork produced from the same single-crystal wafer with a resonance frequency of 55.5 kHz was used in Lancaster<sup>19</sup>. This tuning fork was part of an array of five tuning forks and has the same dimensions  $T$ ,  $W$ , and  $D$ , as the 6.5 kHz fork described above, but its tines are considerably shorter,  $L = 1.20$  mm. The entire array was placed in a square cylinder cell<sup>19</sup> with dimensions  $15 \times 15 \times 21$   $\text{mm}^3$ . The 55.5 kHz tuning fork was used only in its fundamental mode, as the overtone at 340 kHz was severely damped due to acoustic emission<sup>38</sup>, and even at its fundamental resonance, signs of acoustic damping were found. Additionally, the results obtained with another 6.5 kHz fork in Lancaster are presented for comparison.

It ought to be pointed out that these tuning forks were designed specifically to minimize the effects of surface roughness deemed responsible for the irreproducibility of previous experiments. According to the manufacturer’s specifications<sup>58</sup>, the surface roughness is below 1  $\mu\text{m}$  on the original surface of the wafer and about 2  $\mu\text{m}$  on the etched sides. This is a significant improvement over the previously used commercial tuning forks<sup>25</sup>, which have typical surface roughness in excess of 10  $\mu\text{m}$ , with occasional large defects exceeding even 20  $\mu\text{m}$ .

The forks are driven by applying an ac voltage  $V$  from a functional generator to the metallic electrodes deposited on the surface of the quartz. The resulting electric field causes a perturbation in the crystal lattice of the quartz through the piezoelectric effect, which in turn results in a piezo-current  $I$  measured using an IV-converter<sup>42</sup> with a gain of  $10^3$  V/A and a lock-in amplifier. The measurement scheme for the Prague experiment is shown in Fig. 1, the arrangement in the Lancaster experiments was similar, but slightly more complex, as an entire array of five tuning forks (resonating at different frequencies) was connected.

The driving force applied to the fork is given by  $F = aV/2$ , and the velocity of the top of the tines is  $v = I/a$ , where  $a$  stands for the experimentally determined fork constant given by<sup>34,38</sup>:

$$a = \sqrt{\frac{4\pi m_{\text{eff}} \Delta f I}{V}}. \quad (1)$$

Here,  $m_{\text{eff}}$  is the effective mass of the fork at (any) resonance and  $\Delta f$  is the measured width of the resonance. The effective mass of the tuning fork is given by  $m_{\text{eff}} = TWL\rho_q/4$ , where  $\rho_q = 2650$   $\text{kg m}^{-3}$  is the density of the fork material<sup>38</sup>. By performing frequency sweeps

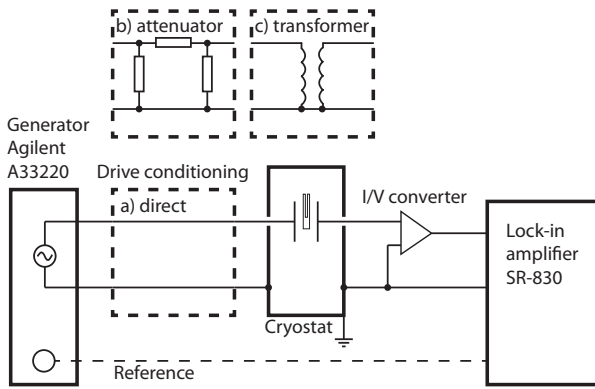


FIG. 1: Diagram of the principal measurement scheme used in Prague. To achieve the full range of velocities, the applied voltage was either a) directly fed to the tuning fork, b) attenuated by one or more inline attenuators, or c) amplified by a transformer with a voltage ratio of 7.31 at the 6.5 kHz fork's fundamental resonance and 2.00 at the overtone. The transformer's output was constantly monitored by a Keithley Model 2000 digital multimeter. An I/V converter<sup>42</sup> with a conversion ratio of 1000 V/A was used to convert the current signal into voltage prior to detection with the SR-830 lock-in.

in vacuum at low temperatures, the experimental fork constants are estimated to be  $a_f = 3.665 \times 10^{-7} \text{ C m}^{-1}$  and  $a_o = 1.409 \times 10^{-6} \text{ C m}^{-1}$  for the fundamental mode and overtone of the 6.5 kHz fork, respectively. For the 55.5 kHz fork, the fork constant of the fundamental mode is given as  $a_f = 9.45 \times 10^{-7} \text{ C m}^{-1}$  in Ref. 38. On resonance, the driving force is balanced by the dissipative drag force acting on the two prongs, so the power dissipated by the fork is equal to the supplied electrical power given by  $\dot{q} = Fv = IV/2$ , using peak values for  $F$ ,  $v$ ,  $I$ , and  $V$ . When obtained from measurements in vacuum, the fork constants are found to be within approximately 10% of the more precise value determined by optical interferometry<sup>43</sup>.

To obtain the best results at low temperatures both in vacuum and superfluid helium, the Prague cell containing the oscillators was flushed repeatedly with dry nitrogen gas prior to cooling. Each time it was pumped down to  $\approx 10^{-5}$  mbar using a turbomolecular pump backed by a membrane pump, simultaneously through the thin (0.2 mm diameter) filling lines and through a direct connection bypassing them. After the last careful evacuation (to  $\approx 10^{-6}$  mbar), the direct connection was closed off. With reasonable confidence that no helium film or any ices could form on the forks at low temperature, the cell was cooled to 10 mK under vacuum. At this point the tuning fork calibration was made. Afterwards, it was filled very slowly over a period of 48 hours with isotopically pure superfluid  $^4\text{He}$ . Similar precautions were taken in the Lancaster experiment as well.

Here, we should also mention that the exact temperature of the tuning fork is, strictly speaking, unknown

during the vacuum measurements, as the fork is thermalized only via its Cu/NbTi leads. However, judging from the properties of the fundamental mode of the 6.5 kHz fork in vacuum (resonant frequency  $f_0 = 6491.3096 \text{ Hz}$ , linewidth  $\Delta f = 0.0082 \text{ Hz}$ ), and in superfluid helium at the temperature of  $\approx 20 \text{ mK}$  (observed linewidth varied between 0.006 and 0.009 Hz), the temperature of the tuning fork does not appear to differ from that of the mixing chamber enough to affect the calibration. Note also the high quality factor of the resonator  $Q = f_0/\Delta f \approx 8 \times 10^5$ . To avoid non-linear behaviour of the oscillator (expected for such a high  $Q$  device), up to 70 dB attenuation was used during the calibration procedure to ensure operation in the linear regime.

### III. EXPERIMENTAL RESULTS

In this section, we present the results obtained in Prague for the 6.5 kHz tuning fork together with a description and estimates of various drag forces acting on the fork under different circumstances. We will only discuss this tuning fork at this point, because it is mostly unaffected by acoustic emission, which simplifies the matter considerably. Traditionally, the obtained results are first shown as the dependence of the peak velocity,  $v$ , on the peak driving force,  $F$ , see Fig. 2. The observed dependencies at the indicated temperatures agree with previous results obtained with the same type of tuning fork to a very good degree<sup>19</sup>. It is important, however, that we are now able to notably extend the range of available velocities using kHz-frequency step up transformers (see Fig. 1).

As expected, the 6.5 kHz tuning fork exhibits linear damping at low velocities at all temperatures. Upon increasing velocities, one or more distinct changes in the force-velocity dependence can be observed occurring at fairly well-defined values of velocity that appear to be independent of temperature,  $T$ , in the studied range  $20 \text{ mK} < T < 1100 \text{ mK}$ . We will analyze these events in greater detail in the following section, and compare our findings with a number of available experiments. Here we start with brief discussion of the linear damping forces observed at low velocities.

The linear damping forces can be fully described and understood as a combination of tuning fork intrinsic damping (dominant at lowest  $T$ ) and ballistic phonon drag ( $\propto T^4$ ), which gradually changes into hydrodynamic viscous damping at higher  $T$ . The relevant dependencies are summarized in Fig. 3, which presents the linear proportionality constant,  $\lambda$ , given by  $F = \lambda v$ . We obtain the value of  $\lambda$  by fitting the linear (low-drive) part of the force-velocity dependence (see Fig. 2). The lower panel of Fig. 3 shows the temperature dependence of the ratio of the  $\lambda$  coefficient obtained for the fundamental mode and the first overtone, denoted as  $\lambda_f$  and  $\lambda_o$ , respectively. At the lowest temperatures, the role of the steeply frequency dependent intrinsic damping is

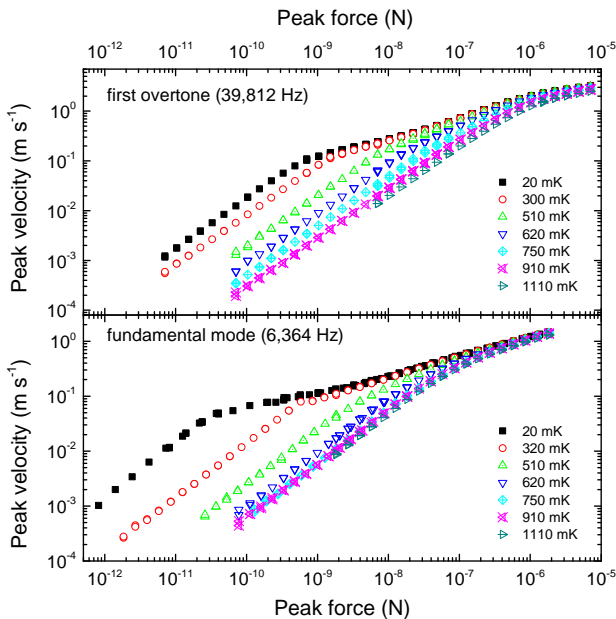


FIG. 2: Peak velocity of the 6.5 kHz tuning fork oscillating at its fundamental frequency (bottom) and at the first overtone (top) as a function of the applied force in helium at various temperatures (color online).

apparent, which likely consists of relatively small losses due to stress-strain hysteresis in the quartz and comparatively larger losses due to sound waves propagating away through the base and leads. We note that sound emission through the surrounding fluid can be safely neglected for the fundamental mode of the tuning fork<sup>37,38</sup> and represents a very small contribution to the overtone damping as well<sup>19</sup>. We will see later that the 55.5 kHz tuning fork displays a measurable acoustic contribution to the drag force, dependent on tuning to or detuning from the acoustic resonances of the surrounding volume.

After examining the linear damping forces acting on the 6.5 kHz fork, we concentrate on experimental data that show non-linear resonant response. It should be noted that unlike previous work with the same tuning fork<sup>19</sup>, we have used full frequency sweeps as a standard measurement technique in the Prague experiment, while amplitude sweeps were used in the Lancaster work. This enables us to monitor all complex features of the resonant responses and examine where the first signs of any type of non-linear behavior occur, whether it is Duffing-like behaviour<sup>44,45</sup>, or the onset of a non-linear drag force. A series of full frequency sweeps taken at 20 mK with the 6.5 kHz fork is shown in Fig. 4. Both the fundamental and overtone modes display Lorentzian resonant responses at the lowest drives and wide flat-top peaks at high drives, due to a non-linear *damping force*. Moreover, in a given range of driving voltages, the fundamental resonance directly displays non-linearities similar to frequency softening in a negative Duffing resonator (c.f.

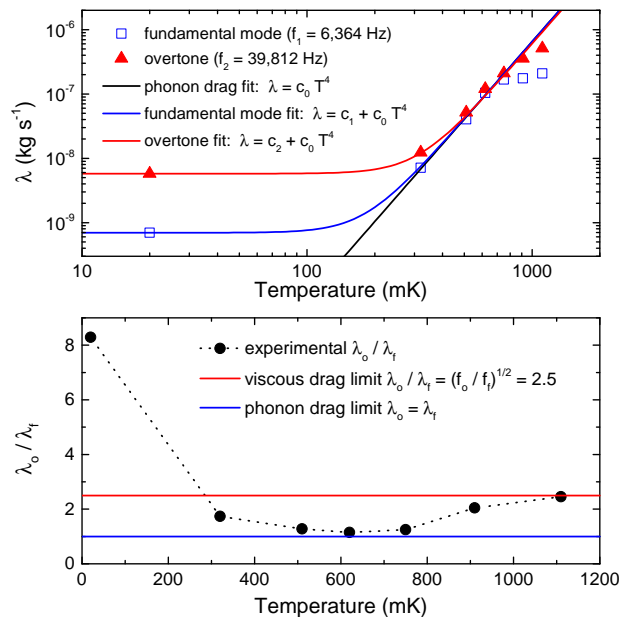


FIG. 3: Analysis of linear drag forces acting on the 6.5 kHz tuning fork with changing temperature. The  $\lambda$  coefficients for the fundamental mode and overtone (at the specified frequencies) are plotted vs. temperature in the top panel. The low-temperature part of each dependence fits well to a sum of ballistic phonon drag ( $\propto T^4$ ) and intrinsic TF damping (constant), while at higher temperatures, deviations occur due to viscous damping from the normal component gradually taking over the part of the ballistic phonon drag. In the lower panel, the ratio  $\lambda_o/\lambda_f$  is shown, highlighting the frequency dependencies of the linear damping in different regimes. The frequency-independent ballistic limit, as well as the viscous limit with square root frequency dependence<sup>39</sup> is clearly indicated.

curves for 83.7  $\mu\text{V}$ , 144  $\mu\text{V}$  and 249  $\mu\text{V}$  in Fig. 4). Note that this type of non-linearity appears before the non-linear drag sets in – without thorough investigation of the shape of the frequency response, this might lead to an incorrect interpretation of the critical velocity (velocities) related to the nucleation of quantized vortices and the eventual production of quantum turbulence. The frequency shifts measured at all temperatures are summarized in Fig. 5. Switching between two metastable states was also observed at intermediate driving voltages, but was not studied systematically within this work.

The values of velocity at which frequency softening, and later non-linear drag, occur are independent of temperature and will be later shown to correspond to the first and second critical velocity as known from other experiments with tuning forks or vibrating grids. Hence we label these values as  $v_{cf1} = 0.02 \text{ m s}^{-1}$  and  $v_{cf2} = 0.06 \text{ m s}^{-1}$  for the fundamental mode, with  $v_{co1} = 0.03 \text{ m s}^{-1}$  and  $v_{co2} = 0.12 \text{ m s}^{-1}$  for the overtone. At this point, we may consider the numerical values only as approximate (determined up to a factor of two); more

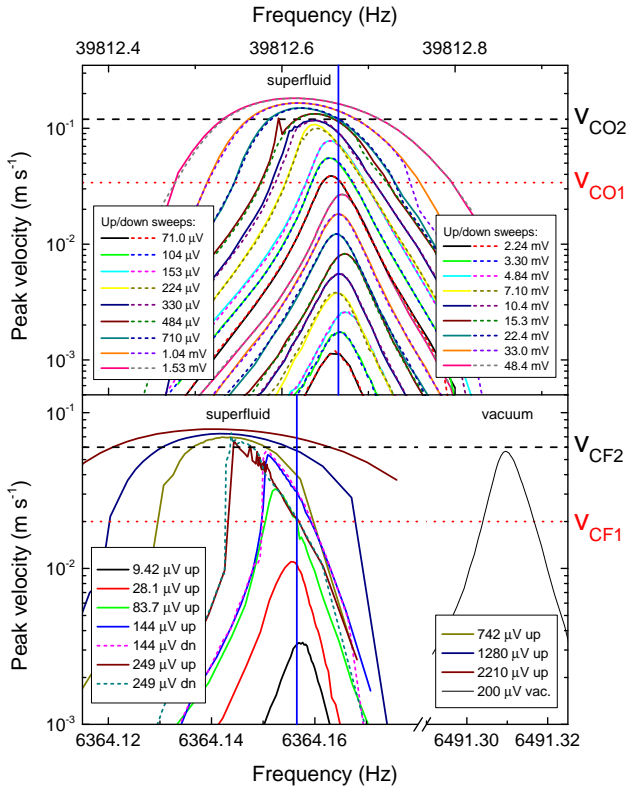


FIG. 4: Selected frequency sweeps of the 6.5 kHz tuning fork at the indicated driving voltages at 20 mK for the fundamental mode (bottom) and overtone (top). The vertical solid blue lines mark the position of the resonance peak at low drives. The red dotted lines estimate the velocity at which the frequency softening sets in for the fundamental mode and the frequency shift becomes apparent for the overtone; the black dashed lines mark estimated velocities at which non-linear damping becomes apparent. Note that the behaviour of the overtone at low drives has almost systematic variations of the resonant frequency. This is not fully understood at this point and is likely related to very weak coupling to resonances of the fork’s mechanical support or to the acoustic resonances of the capillary enclosing the fork. See also Fig. 5 for comparison of the resonance frequencies and Fig. 6 in the next section for the corresponding drag coefficients (color online).

precise values will be given below, as well as a comparison with the 55.5 kHz tuning fork.

#### IV. DISCUSSION – MULTIPLE CRITICAL VELOCITIES

##### A. Prague experiment

The in-line forces acting on an oscillator submerged in a fluid can be divided into a dissipative drag force in-phase with the velocity and an inertial force that is in-phase with the object’s acceleration and does not con-

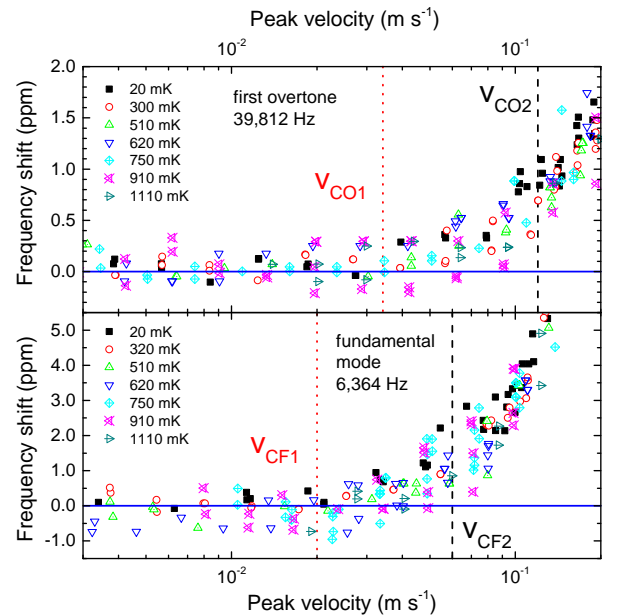


FIG. 5: Resonant frequency shift plotted vs. tuning fork peak velocity for the 6.5 kHz tuning fork (outliers removed). The red dotted lines mark the onset of the shifts in frequency, and coincide with those in Fig. 4; the black dashed lines from Fig. 4 are included for comparison. The horizontal solid blue lines mark zero frequency shift with respect to the resonance at low drives. The onset of the frequency shifts seems to be independent of temperature for either mode in the investigated range. Examples of individual frequency sweeps taken at 20 mK are shown for comparison in Fig. 4 and corresponding drag coefficients can later be found in Fig. 6. The red dotted lines mark the estimated first deviation of the resonance frequency (color online).

tribute to energy dissipation. Examining the results shown above, it should be first noted that the frequency shifts observed above  $v_{cf1}$  or  $v_{co1}$  cannot be explained by any increase in dissipative forces, as dissipation stays approximately constant until  $v_{cf2}$  or  $v_{co2}$  is reached, respectively. Even for higher velocities, a simple estimate yields that the observed frequency shift is roughly one order of magnitude higher than that caused by the increased dissipation. Hence, the resonance peaks are shifted mainly due to a Duffing-like non-linearity, i.e., one related to restoring or inertial forces acting on the fork.

As the elastic and geometric properties of the tuning fork prong are hardly affected at the oscillation amplitudes in question (c.f. vacuum data in Fig. 4), we are left to surmise that it is the hydrodynamic added mass that becomes amplitude-dependent at  $v_{cf1}$  or  $v_{co1}$ . This can be understood in terms of a thin layer of quantized vortex loops “coating” the surface of the tuning fork as suggested before<sup>22,30,31,46</sup>. Through pressure forces, vortex tension, and Kelvin waves, the layer of vortex loops affects the coupling between the oscillator and the fluid, resulting in a gradually changing hydrodynamic added

mass as the oscillation peak velocity (and the number of such vortex loops) is increased. The lack of increase in the drag force suggests that the vortices stay mostly attached to the surface of the fork and do not carry momentum away into the bulk superfluid. Recently, an experiment on vortex pinning at a nearly-spherical protrusion has shown that such pinning can be stable at low flow velocities<sup>47</sup>.

The drag coefficients versus velocity for the fundamental mode and the overtone of the 6.5 kHz tuning fork are plotted in Fig. 6. To calculate the drag  $C_D = 2F/(A\rho v^2)$  from the dissipative force  $F$ , we have assumed that  $A$  equals to the cross-sectional area of a tuning fork prong  $WL$ , that the relevant fluid density is the total density of  $^4\text{He}$  and we use the tuning fork peak velocity for  $v$ .

As in many experiments with submerged oscillators at very low temperatures, we are not able to observe the nucleation of quantized vortices directly through means such as second sound measurements or flow visualization. As the well-established charged vortex ring technique<sup>48</sup> is not available (and would be difficult to use in the given geometry), we have to rely on the drag force measurements as the only indication of the dissipative phenomena occurring in the flow. In practice, this means that the production of quantized vortices becomes apparent in the drag force measurements only when the drag force from the vortices becomes comparable in magnitude to the sum of all pre-existing dissipative forces (such as intrinsic damping, acoustic drag, phonon drag or viscosity). Consequently, all drag force measurements have to be treated with sufficient care, especially when trying to determine critical parameters related to flow instabilities. For example, any critical velocity value determined from these measurements is prone to be overestimated – as we do not necessarily observe the initial instability *per se*, but only the ensuing change in the drag force, when it affects the total of pre-existing drag forces noticeably.

Figures 6 and 7 demonstrate that the onset of non-linear dissipation corresponds very well to the velocities  $v_{cf2}$  and  $v_{co2}$  obtained in our preliminary analysis. The onset velocities again appear to be independent of temperature (see esp. Fig. 7). However, the most important and perhaps surprising result in Fig. 6 is the appearance of a third critical velocity in the overtone drag coefficient, which will be further discussed below. Whether such a critical velocity exists for the fundamental mode cannot be determined with the 6.5 kHz tuning fork, see caption to Fig. 6.

Note that one might be tempted to interpret the bending in the higher temperature data for the fundamental mode as a third critical velocity too. However, this event simply corresponds to the temperature-independent non-linear drag (c.f. Fig. 7) becoming comparable to the linear drag that increases with temperature. Alternatively, flow instabilities occurring in the emerging normal component may be involved as well.

Figure 7 shows the deduced non-linear drag contribution to the damping force, calculated as  $F_{nl} = |F - \lambda v|$

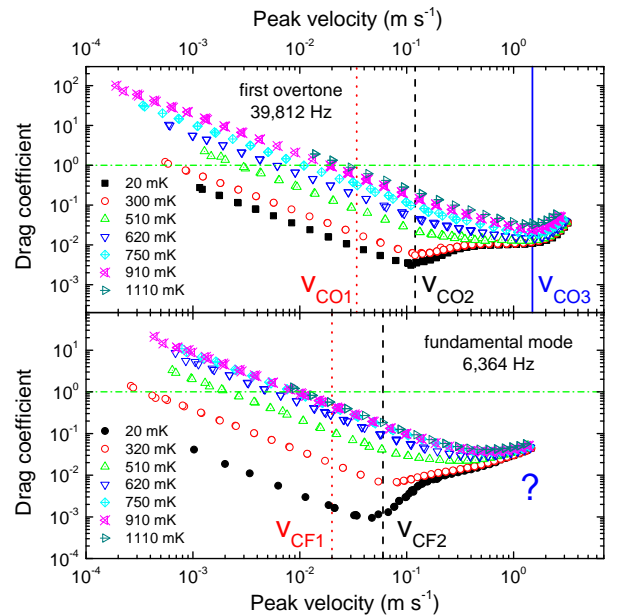


FIG. 6: Dimensionless drag coefficient as a function of peak velocity for the 6.5 kHz tuning fork at various temperatures - fundamental mode (bottom) and overtone (top). Each point is obtained from a full frequency sweep at constant drive. The green dash-dotted horizontal line highlights the value  $C_D = 1$ , while the red dotted and black dashed vertical lines mark the first two critical velocities, respectively, and correspond to the same lines in Figs. 4 and 5. The blue solid line in the overtone drag coefficient (top) shows the value of a third hydrodynamical critical velocity  $v_{co3} = 1.5 \text{ m s}^{-1}$ . The existence of such a third critical velocity for the fundamental mode (bottom) remains unclear, as higher velocities cannot be attained with this tuning fork using the fundamental resonance – the displacement becomes comparable to the prong spacing and at higher drive the two prongs start hitting each other at  $\approx 1.8 \text{ m s}^{-1}$  (color online).

as a function of velocity (the modulus is used to ascertain positive values that can be easily plotted in log scales), illustrating the observed critical velocities in more detail.

Combining the drag coefficient and non-linear force data with our preliminary analysis, we can now determine the critical velocities with improved precision. The corrected critical values for the 6.5 kHz fork and their relative uncertainties are thus:  $v_{cf1} = 0.020 \text{ m s}^{-1}$ ,  $v_{cf2} = 0.060 \text{ m s}^{-1}$ ,  $v_{co1} = 0.034 \text{ m s}^{-1}$  and  $v_{co2} = 0.12 \text{ m s}^{-1}$ , all  $\pm 25\%$ ;  $v_{co3} = 1.5 \text{ m s}^{-1} \pm 35\%$ . The uncertainties are estimated from all the presented graphs, and do not explicitly include the fact that the obtained critical velocities are influenced by our minimum detectable non-linear drag force  $\approx 10^{-10} \text{ N}$  (Fig. 7) and a minimum detectable frequency shift  $\approx 0.5 \text{ ppm}$  for the fundamental mode and  $\approx 0.2 \text{ ppm}$  for the overtone of the 6.5 kHz fork (Fig. 5).

Using the laws of vortex dynamics, it is possible to derive that the critical velocity related to vortex motion and self-reconnections leading to production of additional

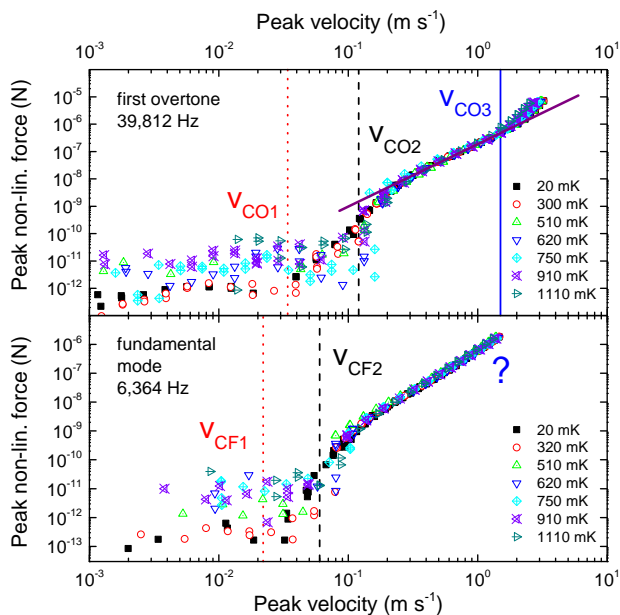


FIG. 7: Peak non-linear drag force (see text) as a function of velocity for the 6.5 kHz tuning fork at the temperatures indicated – fundamental mode (bottom) and overtone (top), with outliers removed. The meaning of lines is the same as in Fig. 6. Additionally, a slanted straight line is used as a guide for the eye; its slope corresponds to a power law with an exponent of approximately 2.3 (color online).

quantized vorticity should scale with the square root of frequency<sup>40</sup>, which would correspond a ratio of  $\approx 2.5$  between the critical velocities for the fundamental mode and the overtone of the 6.5 kHz fork. The observed ratios  $v_{co1}/v_{cf1} \approx 1.7 \pm 0.6$  and  $v_{co2}/v_{cf2} \approx 2.0 \pm 0.7$  (assuming uncorrelated errors of the individual velocities) are in general agreement with this prediction, especially considering the fact that the profile of the overtone flexural mode differs significantly from that of the fundamental resonance. As a result, the overtone mode introduces larger velocity gradients at the same peak velocity, which may affect the process of vortex self-reconnection. Moreover, as we discuss the meaning of the critical velocities later, it becomes obvious that it is the second critical velocity that is related to the onset of significant vorticity production and thus the square root frequency dependence ought to be expected primarily for  $v_{cf2}$  and  $v_{co2}$ .

## B. Lancaster experiment

Recently, investigations of the frequency dependence of critical velocities were carried out by the Lancaster group<sup>19</sup> using, among others, a custom-made tuning fork from the same batch and with the same dimensions as the 6.5 kHz fork presented here. It is therefore natural to compare and combine the results obtained in both

independent experiments and add the data obtained in Lancaster with the 55.5 kHz fork as well. The drag coefficients in Ref. 19 were obtained using amplitude sweeps while tracking the resonance rather than performing full frequency sweeps. A comparison of this measurement technique with full frequency sweeps is presented in the top panel of Fig. 8 for the fundamental mode of the 6.5 kHz fork. The results agree almost perfectly everywhere except near the onset of non-linear dissipation (second critical velocity  $v_{cf2}$ ), where the amplitude sweeps display clear hysteresis, which cannot be detected reliably using full frequency sweeps (see Appendix A).

On the other hand, using amplitude sweeps, the information on frequency shifts of the order of ppm is often lost due to imperfect tracking of the resonance, and thus the very first instability at  $v_{cf1}$  or  $v_{co1}$  is harder to find. The near-perfect agreement between the data obtained in Prague and Lancaster means that the new generation of tuning forks produced for the Lancaster group is indeed capable of providing systematic and reproducible results, which has been one of the main shortcomings of many prior works using oscillating tuning forks.

It should be noted that in the previous Lancaster experiment<sup>19</sup>, the third critical velocity has never been observed with the 6.5 kHz tuning fork, because the data acquired for the first overtone (c.f. Fig. 8 of Ref. 19) did not extend to sufficiently high velocities above  $1 \text{ m s}^{-1}$ . However, the 55.5 kHz tuning fork presented here shows the third critical velocity clearly at a value of approximately  $v_{cf3} = 1.9 \text{ m s}^{-1}$ , see lower panel of Fig. 8. The first two critical velocities were determined as  $v_{cf1} = 0.021 \text{ m s}^{-1} \pm 40\%$ , and  $v_{cf2} = 0.16 \text{ m s}^{-1} \pm 25\%$  for the 55.5 kHz tuning fork in a fashion similar to the procedure for the 6.5 kHz fork. The first critical velocity is, however, less accurate due to the properties of the frequency-tracking algorithm used in the amplitude sweeps.

The first critical velocity appears to be virtually identical between the two different tuning forks here, but our current precision is insufficient to support any claim of frequency-independence, especially recalling the differences between the first critical velocities for the fundamental mode and the overtone of the 6.5 kHz tuning fork (Fig. 5). On the other hand, the square-root frequency scaling for  $v_{cf2}$  predicts a ratio of  $\approx 2.9$  between the 55.5 kHz tuning fork, and the 6.5 kHz one, and the experimental results yield a ratio of  $2.7 \pm 0.9$ , in agreement with the theory. Note also the hysteretic behaviour found at  $v_{cf2}$  for both forks with amplitude sweeps.

Hysteresis at the onset of non-linear dissipation was seen in amplitude sweeps with other types of tuning forks<sup>27</sup>, wires<sup>20,28</sup>, grids<sup>30,31</sup> or spheres<sup>26</sup> and is usually associated with the stochastic onset of (massive) quantized vorticity production. This can be seen as a confirmation that our second critical velocity is indeed related to the production of quantized vortices in such quantities that the resulting drag force is comparable to the intrinsic damping of the oscillator at the given temperature and velocity. The mechanism facilitating this vortex

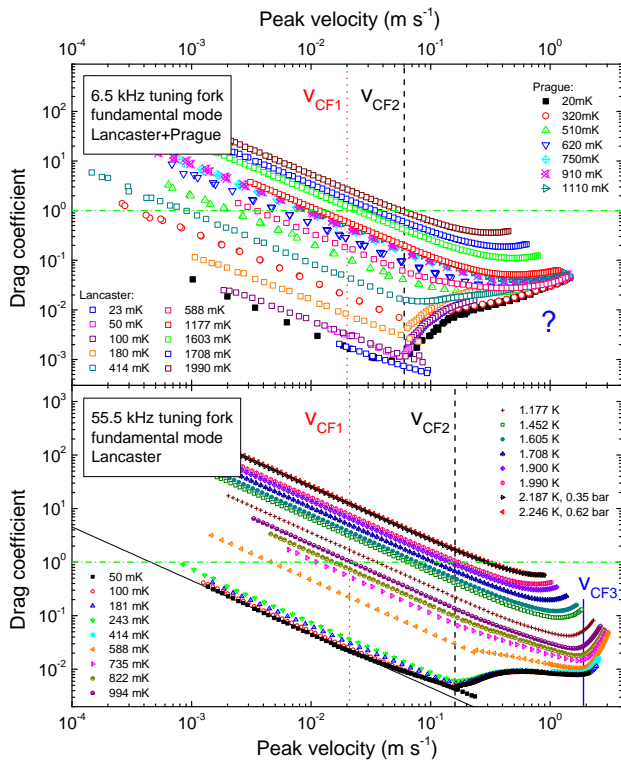


FIG. 8: Top: drag coefficient as a function of velocity measured by amplitude sweeps with resonance tracking in Lancaster and full frequency-sweeps in Prague for the 6.5 kHz tuning fork. While the frequency sweeps are unable to measure the hysteresis at the onset of non-linear dissipation and the amplitude sweeps detect it clearly, the overall reproducibility of the data is surprisingly good, including the values of the second critical velocity. Bottom: drag coefficient as a function of velocity measured by amplitude sweeps with resonance tracking in Lancaster using a 55.5 kHz custom-made tuning fork (dimensions  $T$ ,  $W$ , and  $D$  the same as the 6.5 kHz fork,  $L=1.2$  mm) displaying the third critical velocity in its fundamental mode,  $v_{CF3} = 1.9$   $\text{m s}^{-1}$ , which again appears almost independent of temperature below 1 K. For this tuning fork, the first two critical velocities were determined as  $v_{CF1} = 0.021$   $\text{m s}^{-1}$ , and  $v_{CF2} = 0.16$   $\text{m s}^{-1}$ . In both panels, the green horizontal dash-dotted line marks the value of unity expected for classical flows. Note that at higher temperatures close to the lambda point, the drag coefficient approaches this value at comparatively lower velocities. (color online).

production is likely related to self-reconnections of remnant vortices pinned on the oscillator surface<sup>40,49,50</sup>. It should be emphasized that what is required to observe the non-linear increase in the drag is not just the production of quantized vorticity *per se*, but that this vorticity must actually escape into the bulk, carrying away the momentum provided by the oscillator.

### C. Third critical velocity

Before proceeding with the interpretation of the third critical velocity, several issues need to be addressed. First, measurement and processing artifacts ought to be eliminated. The maximum error in determining the amplitude of a non-linear resonance with respect to a drive- and frequency- dependent background can be estimated to  $\approx 5\%$ , less than the error of the electrical calibration procedure of the tuning fork, and far below the observed effect. Second, while the velocities are, in principle, high enough to warrant risk of cavitation even in superfluid helium<sup>35</sup>, no trace of such an event has been found in the resonance curves of the 6.5 kHz tuning fork, nor in the amplitude response of the 55.5 kHz one. In comparison with previous cavitation studies using tuning forks<sup>35</sup>, the effect on the resonance peak ought to have been even more dramatic here, given the small dimensions of the tuning forks used in this work.

Overheating of the vicinity of the tuning fork can be ruled out as a cause too, as, for example, for the series taken at 20 mK, the temperature in the immediate surroundings of the fork would have to rise significantly to  $\approx 1400$  mK to facilitate such an increase in the drag (see Fig. 6). Given the superb thermal conductivity of superfluid  $^4\text{He}$ , only minimal thermal gradients ought to be present within the fluid inside the Prague or Lancaster cells. While some heating was detected at the mixing chamber stage at the highest tuning fork velocities, it was always around or below 10 mK – too low to consider the experimental cell or parts of it being overheated by more than 1 K. Moreover, the third critical velocity seems to be rather well-defined and almost independent of temperature between 20 mK and 1100 mK, whereas any excessive heating would have to be a smooth function of prong velocity (in contrast to a well-defined critical value) and would become apparent sooner at low temperatures. With all the information available, we are thus led to conclude that the third critical velocity,  $v_{co3}$ , is indeed of hydrodynamical origin.

With the 6.5 kHz fork, we have only observed the third critical velocity using the overtone. One might therefore ask whether it is related specifically to the shape of this particular flexural mode. While it is true that unlike the fundamental mode, the first overtone has two extrema in the velocity profile along the prong length (one at the tip, the other at roughly 45% of the prong length measured from the base), the velocity amplitudes at these maxima are of comparable magnitude<sup>19</sup> as they differ only by a factor of  $\approx 1.5$ . On the other hand, the observed critical velocities differ by a factor of  $v_{co3}/v_{co2} > 10$ , making any direct connection between nucleation of vorticity at the other velocity profile maximum and the observed third critical velocity highly improbable.

The experimental fact that the third critical velocity was also observed with the fundamental mode of the 55.5 kHz fork is of course, another, and much stronger argument supporting the notion that the exact resonant

mode used is irrelevant to the observation of the third critical velocity. Moreover, previous work<sup>19</sup> indicates that the critical velocities are governed mainly by the tips of the tuning fork prongs and that they seem to be largely insensitive to the velocity profile along the prongs. In summary, the third critical velocity seems to be temperature-independent, related to superfluid hydrodynamics and has been found independently and reproducibly with two different carefully designed and prepared tuning forks, in two different laboratories using two different measurement techniques.

#### D. Comparison with previous experiments

Past experiments<sup>22,30</sup> that observed two critical velocities with oscillators in superfluid  $^4\text{He}$  were usually interpreted in such a manner that the first critical velocity corresponds to the formation of a layer of quantized vorticity near the surface of the oscillator in question, without dissipating much energy in the process. The second critical velocity was then usually thought to correspond to the spreading of quantized vortices into the bulk in the form of emitted vortex loops and/or to the formation of a partly polarized turbulent vortex tangle producing large eddies at length scales exceeding the mean intervortex spacing - the *quantum length scale*. Note in passing that a similar scenario has been expected to work<sup>50</sup> not only in the zero temperature limit, but also in the two-fluid regime at finite temperature above about 1 K.

##### 1. Tuning forks

Of all the experimental results available today, we first discuss the work in Ref. 22 with tuning forks in isotopically pure  $^4\text{He}$ . These measurements have been taken with several tuning forks placed in different enclosures inside a large experimental cell mounted on the mixing chamber of the dilution refrigerator. All of the forks have clearly displayed significant acoustic emission, which was lowest for the 32 kHz tuning fork labeled “F1” placed inside its original capsule with only a tiny 0.4 mm opening. This tuning fork displayed two critical velocities with values of  $v_{c1} = 0.006 \text{ ms}^{-1}$  and  $v_{c2} = 0.1 \text{ ms}^{-1}$ , respectively.

In the cited work,  $v_{c2}$  is interpreted as a full-fledged transition to quantum turbulence, while  $v_{c1}$  is discussed speculatively; a relation to the formation of a pseudo-viscous flow in the vicinity of the oscillator is proposed. Comparing the observed values with our critical velocities, we find that  $v_{c2}$  is close with our second critical velocities ( $v_{cf2} = 0.060 \text{ ms}^{-1}$ ;  $v_{co2} = 0.12 \text{ ms}^{-1}$  for our 6.5 kHz fork;  $v_{cf2} = 0.16 \text{ ms}^{-1}$  for our 55.5 kHz fork), especially after taking into account the expected scaling with the square root of frequency<sup>40</sup>. We are therefore led to believe that the flow instabilities occurring at all of these velocities are of the same nature. We note that the

third critical velocity has not been observed in Ref. 22 despite having reached velocities close to  $2 \text{ ms}^{-1}$  with their 32 kHz fork labeled “f3”.

On the other hand, we have not observed any sign of such effects as seen in Ref. 22 around their  $v_{c1}$ , notably the increase or suppression of the drag depending on whether the original value of the drag was high or low (as influenced by coupling to acoustic modes) with our 6.5 kHz tuning fork. As this fork was designed and chosen with special considerations for minimizing its acoustic emission, it seems that the effects observed in Ref. 22 might be related to acoustics phenomena. Indeed, the 55.5 kHz fork that is expected to have a measurable acoustic drag shows such an increase in the drag force (Fig. 8).

It seems very likely that the resonant frequency of the forks used in Ref. 22 has shifted slightly, as for our forks above the first critical velocity. This may be caused by formation of a thin vortical layer near the tuning fork, as the authors discuss in their work. This shift in frequency would have affected the tuning to/detuning from the acoustic resonances of the surrounding volume. We contacted Deepak Garg, the principal author of Ref. 22, who sent us a sample of resonant frequency data. These data show a gradual downward frequency shift starting around their  $v_{c1}$  and going down by 2.5 ppm before reaching  $v_{c2}$ , although it might also be affected by the frequency drifting due to acoustic coupling. We are therefore left to surmise that the change in drag at  $v_{c1}$  observed in Ref. 22 and also with our 55.5 kHz fork is likely due to a change in the acoustic dissipation.

##### 2. Tuning forks and microwires

Next, we compare our data with those of Bradley and co-workers obtained in superfluid  $^4\text{He}$  at mK temperatures with oscillating wires<sup>20</sup> and forks<sup>21</sup>. With both types of devices, they observed a velocity,  $v_{\text{onset}}$ , above which extra turbulent drag is detected. For each device, this velocity was irreproducible from one sweep to the next and behaved stochastically. Therefore, for each device, the authors clearly defined a critical velocity  $v_{c1}$  by extrapolating to zero turbulent drag. This velocity was reproducible between sweeps and corresponded to the minimum velocity needed to produce and sustain the vortex lines that create drag forces.

Additionally, for each device, the authors identified another reproducible critical velocity  $v_{c2}$  above which the drag rises much more steeply. The magnitudes of the two characteristic velocities obtained for the 32 kHz tuning fork were very close<sup>21</sup>:  $v_{c1} \approx 0.053 \text{ ms}^{-1}$  and  $v_{c2} \approx 0.056 \text{ ms}^{-1}$ . For the wires resonating at  $\approx 1 \text{ kHz}$ , values  $v_{c1} \approx 0.035 \text{ ms}^{-1}$ , and  $v_{c2} \approx 0.060 \text{ ms}^{-1}$  or  $v_{c2} \approx 0.075 \text{ ms}^{-1}$  were found<sup>20</sup>, depending on the exact wire and frequency used. Again, the higher critical velocity is tentatively linked to the massive production of quantized vortices resulting in developed quantum turbu-

lence, while the lower one is considered a limiting value above which drag-inducing quantized vortices can only be sustained.

These results differ from ours in the sense that the first critical velocity already marks some (albeit small) increase of dissipation, whereas in our case the flow continues to be dissipationless (within our resolution) in the narrow range of velocities between our first and second critical velocity (although a weak increase in dissipation could be argued for the data taken at 20 mK, see Fig. 7). Frequency shifts have been observed in Refs. 20, 21 above their first critical velocity, too. It is also important that the values of the drag coefficient near and above the observed critical velocities were very low in Refs. 20, 21, one to two orders of magnitude below unity. The observed turbulent drag therefore does not resemble classical turbulent drag.

### 3. Grids

Similar experiments with grids oscillating at  $\approx 1$  kHz in  $^4\text{He}$  have shown comparable results<sup>30</sup>, and again, two critical velocities have been observed, this time with values  $v_{g1} \approx 0.003 \text{ m s}^{-1}$  and  $v_{g2} \approx 0.03 \text{ m s}^{-1}$ . The first critical velocity for the grid was accompanied with a pronounced frequency shift (no increase in drag), interpreted as extra hydrodynamical added mass due to a boundary layer of quantized vortices, while the second clearly marked the onset of extra dissipation. This seems consistent with Refs. 20–22 and our work, and highlights the frequency shift needed to observe the change in acoustic damping in Ref. 22 or with our 55.5 kHz tuning fork.

As far as the actual values of the first critical velocity are concerned, assuming that it is indeed related to a formation of a vortical layer on the surface of the oscillator which affects the hydrodynamic added mass, one might expect the critical velocity to depend on the surface quality of the oscillator in question. The grid has relatively large micron-scale ( $\approx 20 \mu\text{m}$  bar width and  $\approx 127 \mu\text{m}$  mesh size) features everywhere, so the formation of the boundary layer might be the easiest – observed at the lowest velocity. While we have no direct measure of the surface quality of the tuning fork “F1” in Ref. 22 or the fork in Ref. 21, these are commercially produced devices, which typically have surface roughness of order  $10 \mu\text{m}$  or even higher<sup>25</sup>. Our custom-made tuning forks have a significantly better surface quality ( $< 2 \mu\text{m}$ ), and the surface roughness of the micron-sized wires is probably below  $1 \mu\text{m}$ . This might explain why the tuning forks and wires detect no frequency shift due to vortices pinned on the surface at such low velocities as  $v_{g1} \approx 0.003 \text{ m s}^{-1}$ , but instead at velocities roughly one order of magnitude higher.

### 4. Experiments with oscillators - summary

Collecting evidence from all the above-mentioned experiments, we are led to believe that the first (lowest) critical velocity observed in all the experiments is of hydrodynamic origin and is indeed related to the formation of a vortical boundary layer which can be expedited by larger surface features on the device used. The second critical velocities from Refs. 22,30 correspond to our second critical velocity too, and can be linked reliably to significant production of quantized vorticity which then propagates away from the surface of the oscillator, as it always features a rapid increase in the drag force and hysteresis (if measured using amplitude-sweeps)<sup>19–22</sup>.

After exceeding the second critical velocity, the values of the drag coefficient are typically of the order  $10^{-2}$  or  $10^{-1}$  across our work and the referred experiments. This suggests that flow patterns significantly different from classical turbulence are present. In classical oscillatory flows, drag coefficients of order unity are expected for cylinders or tuning forks<sup>17,18,25</sup> at sufficiently high Reynolds number (or Keulegan-Carpenter number), where the pressure drag is dominant. Thus, we believe that no large flow structures resembling the classical wake exist in the superflow above the second critical velocity yet, and that our newly observed third critical velocity, above which the drag coefficient starts rising towards unity, may be related to a distinct change in the flow pattern, in which the superfluid develops larger polarized structures and starts to mimic the behavior of classical turbulent flows. This scenario is also supported by order-of-magnitude estimates of vortex line density provided in Appendix B.

It should be noted that at higher temperatures approaching  $T_\lambda = 2.17 \text{ K}$ , the drag coefficients obtained with our tuning forks approach unity at velocities notably below  $v_{cF3}$  (c.f. Fig. 8). This suggests that larger vortical structures present in the (transitional or turbulent) flow of the normal component affect the drag considerably, and perhaps also induce the superfluid component to mimic classical behaviour already at lower velocities, via the action of the mutual friction force as suggested in Ref. 25. Mutual friction is directly related to the density of quantized vortices and is thus expected to arise already above the second critical velocity, which is in our case roughly one order of magnitude lower.

If our scenario is correct, the possibility to observe the third critical velocity would likely depend on the exact geometry of the flow, specifically on the range of length-scales at which the flow is driven. Experiments with floppy grids<sup>23</sup> or large commercial tuning forks<sup>24</sup> (tine length 3.9 mm, cross-section 0.39 mm by 0.28 mm) that show drag coefficients of order unity in the zero temperature limit without any explicit cross-over from the “ultra-quantum” to the “quasi-classical” regime are in fact good examples of flows driven at large scales (grid or fork dimensions) and small scales (mesh size, surface roughness) at the same time. On the other hand, drag coefficients

significantly below unity are found in experiments where the flow is driven predominantly at small scales, e.g. with the much smaller tuning forks custom-made for the Lancaster group<sup>19</sup> that are used in this work too, vibrating wires<sup>20</sup>, or the oscillating grid<sup>30,31</sup>. The electrostatically driven grid is included in this group because it does not move translationally or act as a solid bluff body; it thus drives the flow mainly at the scales of the mesh size or bar width.

The last group of experiments<sup>21,22</sup>, using relatively large commercial tuning forks, but not observing drag coefficients of order unity can very likely be understood as simply having an insufficient maximum velocity ( $\approx 0.8 \text{ m s}^{-1}$  for fork “F1” in Ref. 22, and  $\approx 0.5 \text{ m s}^{-1}$  for the forks in Ref. 21) for the classical-like flow pattern to emerge or to manifest in the drag coefficient. In the end, whether all three critical velocities are observed distinctly or whether they coincide seems to be determined by the surface quality of the given oscillator and by the length scales at which the flow is driven. We believe that this is the reason why it has been extremely difficult to find significant common ground between the numerous experiments with submerged oscillators performed in the last two decades.

## V. CONCLUSIONS

We have investigated instabilities in oscillatory flow due to tuning forks in isotopically pure superfluid helium, focusing on the zero temperature limit. We have analyzed linear damping at low drives and ascertained that acoustic radiation into the fluid can be neglected for the 6.5 kHz tuning fork operated at its fundamental and first overtone modes, while it is measurable for the 55.5 kHz tuning fork. Apart from the two critical velocities known from earlier work, we have observed a previously unknown third hydrodynamic critical velocity, which we associate with the predominantly “ultra-quantum” turbulence (characterized by the quantum length scale – the mean intervortex distance) developing larger coherent structures and starting to mimic the behavior of classical fluids. For the tuning forks used, this behaviour was most clearly expressed at the lowest attainable temperature of 20 mK.

Here, we propose a tentative explanation linking all the observations of oscillatory flow in zero temperature limit into a single framework. Specifically, we suggest that the first critical velocity, connected mostly to frequency shifts rather than changes in the drag force, is associated with the formation of a number of quantized vortex loops near the surface of the oscillator, possibly forming a thin layer, which affects the coupling to the fluid and thus the hydrodynamic added mass. We believe that the value of this first critical velocity is strongly dependent on the surface quality of the given oscillator; smoother surfaces are likely to result in a higher value, as one might expect from considerations of ideal flow enhancement past sharp

corners. The second critical velocity is then related to the quantized vorticity propagating into the bulk of the superfluid, either in the form of emitted vortex loops or, eventually, as a turbulent tangle. It is always accompanied by a marked increase in the drag force and usually hysteresis (detectable with amplitude sweeps). The third and highest critical velocity, above which the drag coefficient starts to grow towards unity, was found to be hydrodynamic in origin. We propose that it is linked to a qualitative change in the pattern of quantized vorticity, during which the vortex tangle becomes partly polarized, developing larger structures, and on scales exceeding the quantum length scale starts to mimic classical turbulence generated by oscillating objects in viscous fluids.

We note that at higher temperatures in the two-fluid regime, the situation is far more complex due to the possibility of the superfluid and normal component flows becoming unstable independently and due to the mutual friction force coupling their velocity fields. This represents a significant challenge for future research and we hope that our work will provide a useful stepping-stone for such an endeavour.

## Acknowledgments

We thank Deepak Garg for sending us the original data of Ref. 22 as well as E. Zemina and B. Vejr for technical assistance. This work is supported by the Czech Science Foundation under project GACR 203/14/02005S, by UK EPSRC grant EP/L000016/1, and by the European Community Framework Programme 7, EuHIT - European High-performance Infrastructures in Turbulence, grant agreement no. 312778. DS acknowledges institutional support under UNCE 2040.

## APPENDIX A: MEASUREMENT TECHNIQUES

Experimentalists working with sensitive high-Q resonators at mK temperatures often have to deal with the extremely long times it takes for such oscillators to stabilize at a given drive level and frequency. For example, for the 6.5 kHz fork, the vacuum linewidth,  $\Delta f_0$  was about 8 mHz, meaning that the relaxation time  $\tau = 1/\Delta f_0$  amounts to 125 s. For example, if the waiting between individual points on a frequency sweep is set to roughly three times the relaxation time (375 s), the entire f-sweep, comprising of 100 points, would take over 10 hours. For these reasons it is often impractical to use frequency sweeps for the studies of the transition to quantum turbulence, as each force-velocity curve for a given setting of the driving voltage would take a considerable amount of time, at least until turbulence is produced and the linewidth increases significantly.

There are, however, some aspects of the resonance that cannot be found without performing full frequency sweeps (and optimizing for speed wherever possible). In

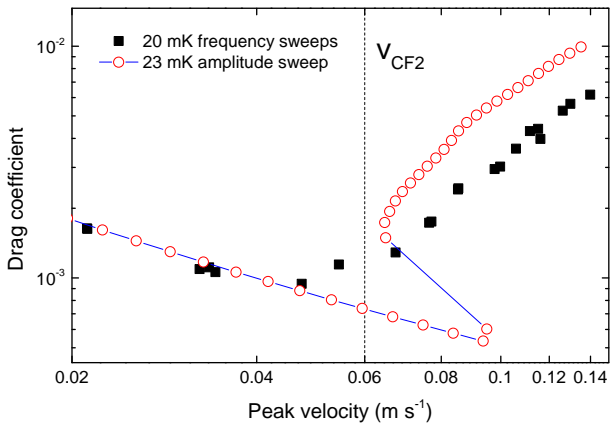


FIG. 9: Comparison of the low temperature drag coefficient velocity-dependence of the fundamental mode of the 6.5 kHz tuning fork measured by amplitude sweeps and a series of frequency-sweeps. The second critical velocity is indicated by the vertical dashed line. Note that the data measured using the amplitude sweeps show hysteresis (color online).

Fig. 9 we present a direct comparison of the results obtained near  $v_{cf2}$  on the 6.5 kHz tuning fork using amplitude sweeps with resonance tracking and full frequency sweeps. While using the amplitude sweeps helps uncover the hysteresis at the transition (which is inaccessible with frequency sweeps, as the tuning fork velocity varies during each sweep), the non-linear resonance will only be revealed when using full frequency sweeps, as the tiny shifts in resonance frequency are difficult to detect with a resonance-tracking amplitude sweep algorithm.

Recently, a new technique has been tested for the measurement of resonant responses that promises to become a powerful combination of both approaches – the multi-frequency lock-in technique<sup>51</sup>. Significant improvements in acquisition times have been demonstrated in the linear mode of tuning forks at room temperature ( $Q \approx 3000$ ) and first measurements have been made in superfluid  $^4\text{He}$  above 1.4 K with promising results. The performance of this technique at mK temperatures is yet to be tested carefully, especially bearing in mind the extremely good quality factors of order  $10^5$  or  $10^6$  and the various types of non-linearities present in the flow past oscillating bodies in superfluid helium.

## APPENDIX B: ESTIMATES RELATED TO CRITICAL VELOCITIES

Here we estimate the effects due to quantized vortices (QVs) near the second and third critical velocities obtained with the 6.5 kHz and 55.5 kHz tuning forks. We begin by estimating the superfluid mass effectively coupled to the resonators near the second critical velocity from the measured frequency shifts. For the 6.5 kHz tuning fork, we have shifts of 1.5 ppm at  $v_{cf2}$  and 0.8 ppm

at  $v_{co2}$ ; for the 55.5 kHz fork we have 1.1 ppm at  $v_{cf2}$ . This leads to absolute effective mass enhancements of order  $10^{-14}$  kg, corresponding to a layer of superfluid helium near the surface of the fork, of thickness  $\approx 2 \text{ \AA}$ . This amount of helium is coupled to the oscillator through the action of QVs and Kelvin waves (KWs), in excess of the fluid already coupled due to potential flow past the fork. This thickness is in fact very close to the vortex core size<sup>52</sup> (likely a numerical coincidence) and it shows that any additional coupling of the oscillator to the surrounding superfluid due to QVs is very weak.

Estimating the radius of a vortex loop,  $r$ , satisfying the fundamental resonance condition for KW excitations<sup>53</sup> at the given frequencies yields values of order  $10^{-7}$  m. A very crude estimate of a semi-circular QV loop effective hydrodynamic mass can be made based on the momentum of a free vortex ring<sup>54</sup>,  $p = \rho_S \kappa \pi r^2$ , and the induced superfluid velocity in its center,  $v_S = \kappa / (2r)$ . Such a simple estimate leads to numbers of vortex loops pinned on the surface of the fork between approximately 50 (6.5 kHz fork) and 1000 (55.5 kHz fork), just below the second critical velocity. The mean distance between pinned loops exceeds  $r$  by almost two orders of magnitude, hence interactions between loops should be statistically insignificant. These estimates are in general agreement with our tentative interpretation that relatively few QVs are attached to the surface and that they likely do not extend far into the surrounding superfluid.

Next, we proceed to estimate the vortex line density needed to dissipate the power input into the fluid by the resonator near the third critical velocity. We will use two different approaches: one based on the dissipation of unpolarized (unstructured) vortex line density as given by the Vinen equation; the other following a classical description of turbulent flow. In a stationary case, the total power dissipated by the flow must be equal to the power supplied to the tuning fork, given by  $\dot{q} = IV/2 = Fv$ , see Section II. If our interpretation is correct, at the third critical velocity the dissipation due to classical-like (structured) flow,  $P_C$  should become comparable to the one dissipated through the ultra-quantum (unstructured) vorticity,  $P_Q$ . For the sake of the argument, we will use  $P_C = P_Q = \dot{q}/2$ .

To convert the supplied power to energy dissipation per unit volume, we need to know an effective volume wherein this power is dissipated. Using the size of a container or an experimental cell would clearly lead to unphysical results, unless its dimensions were comparable to those of the tuning fork. Instead, we choose two physically relevant volumes for comparison. The first choice,  $V_1$ , is determined by the tuning fork dimensions, as these are relevant to the velocity field of ideal flow past the fork. We thus define an elliptical cylinder encapsulating the tuning fork, with lateral dimensions  $2a = 3W$ ,  $2b = D + 4T$  and height  $h = L$ , and subtract the volume of the fork itself. The second option,  $V_2$ , is chosen as a thin layer near the surface of the fork with its thickness given by the radius of vortex loops  $r$ . We consider these to be

the extreme cases, in reality the volumes differ by three orders of magnitude and the actual dissipating volume will likely be in between.

For an unpolarized bundle, the dissipation of vortex line density is given by the Vinen equation (see Ref. 55, Eq. 30) as  $dL/dt = -\kappa L^2/(2\pi)$ , ignoring the factor  $\chi_2$  of order unity. The energy of unpolarized vortices can be estimated as the sum of individual vortex energies and is given in Ref. 56, Eq. (29). Using these two relations and equating the energy dissipation per unit volume to  $P_Q/V_1$ , the unpolarized vortex line density can be estimated as  $L_\times \approx 2.5 \times 10^{11} \text{ m}^{-2}$  and  $3.3 \times 10^{11} \text{ m}^{-2}$ , for the 6.5 kHz and 55.5 kHz forks, respectively. Using  $P_Q/V_2$ , we get  $L_\times \approx 5.5 \times 10^{12} \text{ m}^{-2}$  and  $9.4 \times 10^{12} \text{ m}^{-2}$ .

On the other hand, Kolmogorov's treatment of classical turbulence estimates the kinetic energy flux per unit volume as  $\rho u^3/(2d)$ , with  $u$  being the characteristic velocity of large, energetic eddies and  $d$  their dimension. Based on the visualization of oscillatory flow of superfluid  $^4\text{He}$  past a rectangular cylinder in Ref. 57, Fig. 3, we choose  $d = W/2$ . Equating the energy dissipation to  $P_C/V_1$  gives eddy velocities of  $47 \text{ mm s}^{-1}$  and  $57 \text{ mm s}^{-1}$  for the 6.5 kHz and 55.5 kHz tuning fork, respectively. Assuming solid body rotation of the large eddy and full polarization of QVs, the corresponding vortex line density is given by  $L_\parallel = 4u/(\kappa d)$ . This leads to values  $L_\parallel \approx 8.5 \times 10^{10} \text{ m}^{-2}$  and  $1.0 \times 10^{11} \text{ m}^{-2}$ , for the 6.5 kHz and 55.5 kHz forks,

respectively. Using  $P_C/V_2$ , we get  $L_\parallel \approx 6.3 \times 10^{11} \text{ m}^{-2}$  and  $8.9 \times 10^{11} \text{ m}^{-2}$ . It is remarkable that if we attempt to estimate the Kolmogorov length scale as  $\eta = (\kappa^3/\epsilon)^{1/4}$ , with  $\epsilon = u^3/d$ , and compare it to the mean inter-vortex distances obtained using both approaches,  $\delta_\times = 1/\sqrt{L_\times}$  and  $\delta_\parallel = 1/\sqrt{L_\parallel}$ , we always find that  $\delta_\times < \eta < \delta_\parallel$  and for a given choice of the effective volume, all the values fall within a factor of three.

In all cases, a larger density is found for unpolarized vortices:  $L_\times > L_\parallel$ , as might be expected, but the values are within one order of magnitude. We stress that this is not universal behaviour of the model and depends on the total amount of energy dissipated per unit volume. The actual values of  $L$  are somewhat higher than measured in a steady flow of superfluid  $^4\text{He}$  at 1.6 K with a mean flow velocity of  $\approx 1 \text{ ms}^{-1}$  in Ref. 56, which states a value of  $L = 6 \times 10^{10} \text{ m}^{-2}$ . This can be expected, as our case differs in three important aspects: (i) lower temperatures and little or no dissipation due to mutual friction, (ii) oscillatory flow, where the body moves through its wake and interacts with vortices, and (iii) higher characteristic velocity ( $1.5$  and  $1.9 \text{ m s}^{-1}$ ). While these rough estimates are of speculative nature, it seems that the third critical velocity may indeed be related to a situation where polarized, classical-like vortex structures start to manifest in a predominantly quantum flow.

- 
- <sup>1</sup> W. F. Vinen, in *Progress in Low Temperature Physics*, vol. III, p. 1, edited by Gorter, C. J., North-Holland Publications, Amsterdam (1961).
- <sup>2</sup> C. F. Barenghi, R. J. Donnelly, W. F. Vinen (editors), *Quantized Vortex Dynamics and Superfluid Turbulence*, LNP 571, Springer-Verlag Berlin Heidelberg, 2001.
- <sup>3</sup> M. La Mantia, L. Skrbek, *Europhys. Lett.* **105**, 46002 (2014).
- <sup>4</sup> E. Varga, S. Babuin, L. Skrbek, *Phys. Fluids* **27**, 065101 (2015).
- <sup>5</sup> S. Babuin, E. Varga, L. Skrbek, E. Lévêque, P.-E. Roche, *Eur. Phys. Lett.* **106**, 24006 (2014).
- <sup>6</sup> P. M. Walmsley, A. I. Golov, H. E. Hall, A. A. Levchenko, W. F. Vinen, *Phys. Rev. Lett.* **99**, 265302 (2007).
- <sup>7</sup> D. E. Zmeev, P. M. Walmsley, A. I. Golov, P. V. E. McClintock, S. N. Fisher, W. F. Vinen, *Phys. Rev. Lett.* **115**, 155303 (2015).
- <sup>8</sup> L. K. Sherwin-Robson, C. F. Barenghi, A. W. Baggaley, *Phys. Rev. B* **91**, 104517 (2015).
- <sup>9</sup> A. W. Baggaley, V. Tsepelin, C. F. Barenghi, S. N. Fisher, G. R. Pickett, Y. A. Sergeev, N. Suramlishvili, *Phys. Rev. Lett.* **115**, 015302 (2015).
- <sup>10</sup> W. F. Vinen, *Phys. Rev. B* **61**, 1410 (2000).
- <sup>11</sup> A. W. Baggaley, C. F. Barenghi, A. Shukurov, Y. A. Sergeev, *Euro. Phys. Lett.* **98**, 26002 (2012).
- <sup>12</sup> C. F. Barenghi, L. Skrbek, K. R. Sreenivasan, *Proc. Natl. Acad. Sci. U.S.A.* **111**, suppl. 1, 4647-4652 (2014).
- <sup>13</sup> W. F. Vinen, L. Skrbek, *Proc. Natl. Acad. Sci. U.S.A.* **111**, suppl. 1, 4699-4706 (2014).
- <sup>14</sup> W. Guo, M. La Mantia, D. P. Lathrop, S. W. Van Sciver, *Proc. Natl. Acad. Sci. U.S.A.* **111**, suppl. 1, 4653-4658 (2014).
- <sup>15</sup> P. Walmsley, D. Zmeev, F. Pakpour, A. Golov, *Proc. Natl. Acad. Sci. U.S.A.* **111**, suppl. 1, 4691-4698 (2014).
- <sup>16</sup> L. Skrbek, W. F. Vinen, *The use of vibrating structures in the study of quantum turbulence*, in *Progress in Low Temp. Phys.*, edited by M. Tsubota and W. P. Halperin (Elsevier, Amsterdam, 2009), Vol. XVI, Chap. 4.
- <sup>17</sup> P. W. Bearman, M. J. Downie, J. M. R. Graham, E. D. Obasaju, *J. Fluid Mech.* **154**, 337-356 (1985).
- <sup>18</sup> T. Sarpkaya, *J. Fluid Mech.* **165**, 61 (1986).
- <sup>19</sup> S. L. Ahlstrom, D. I. Bradley, M. Človečko, S. N. Fisher, A. M. Guénault, E. A. Guise, R. P. Haley, O. Kolosov, P. V. E. McClintock, G. R. Pickett, M. Poole, V. Tsepelin, A. J. Woods, *Phys. Rev. B* **89**, 014515 (2014).
- <sup>20</sup> D. I. Bradley, S. N. Fisher, A. M. Guénault, R. P. Haley, V. Tsepelin, G. R. Pickett, K. L. Zaki, *J. Low Temp. Phys.* **154**, 97 (2009).
- <sup>21</sup> D. I. Bradley, M. J. Fear, S. N. Fisher, A. M. Guénault, R. P. Haley, C. R. Lawson, P. V. E. McClintock, G. R. Pickett, R. Schanen, V. Tsepelin, L. A. Wheatland, *J. Low Temp. Phys.* **156**, 116-131 (2009).
- <sup>22</sup> D. Garg, V. B. Efimov, M. Giltrow, P. V. E. McClintock, L. Skrbek, W. F. Vinen, *Phys. Rev. B* **85**, 144518 (2012).
- <sup>23</sup> D. I. Bradley, S. N. Fisher, A. M. Guénault, R. P. Haley, M. Kumar, C. R. Lawson, R. Schanen, P. V. E. McClintock, L. Munday, G. R. Pickett, M. Poole, V. Tsepelin, P. Williams, *Phys. Rev. B* **85**, 224533 (2012).
- <sup>24</sup> G. A. Sheshin, A. A. Zadorozhko, E. Ya. Rudavskii, V. K. Chagovets, *Low Temp. Phys.* **34**, 875 (2008).

- <sup>25</sup> M. Blažková, D. Schmoranzer, L. Skrbek, W.F. Vinen, *Phys. Rev. B* **79**, 054522 (2009).
- <sup>26</sup> J. Jäger, B. Schuderer, W. Schoepe, *Phys. Rev. Lett.* **74**, 566 (1995).
- <sup>27</sup> D. I. Bradley, M. J. Fear, S. N. Fisher, A. M. Guénault, R. P. Haley, C. R. Lawson, G. R. Pickett, R. Schanen, V. Tsepelin, L. A. Wheatland, *J. Low Temp. Phys.* **175**, 379-384 (2014).
- <sup>28</sup> H. Yano, T. Ogawa, A. Mori, Y. Miura, Y. Nago, K. Obara, O. Ishikawa, T. Hata, *J. Low Temp. Phys.* **156**, 132 (2009).
- <sup>29</sup> D. I. Bradley, A. M. Guénault, S. N. Fisher, R. P. Haley, M. J. Jackson, D. Nye, K. O'Shea, G. R. Pickett, V. Tsepelin, *J. Low Temp. Phys.* **162**, (2011) 375.
- <sup>30</sup> H. A. Nichol, L. Skrbek, P. C. Hendry, P. V. E. McClintock, *Phys. Rev. E* **70**, 056307 (2004).
- <sup>31</sup> H. A. Nichol, L. Skrbek, P. C. Hendry, P. V. E. McClintock, *Phys. Rev. Lett.* **92**, 244501 (2004).
- <sup>32</sup> V. Strouhal, *Annalen der Physik und Chemie*, 3rd series, **5**(10), 216 (1878).
- <sup>33</sup> M. Blažková, D. Schmoranzer, L. Skrbek, *Phys. Rev. E* **75**, 025302 (2007).
- <sup>34</sup> R. Blaauwgeers, M. Blažková, M. Človečko, V. B. Eltsov, R. de Graaf, J. J. Hosio, M. Krusius, D. Schmoranzer, W. Schoepe, L. Skrbek, P. Skyba, R.E. Solntsev, D.E. Zmeev, *J. Low Temp. Phys.* **146**, 537 (2007).
- <sup>35</sup> M. Blažková, T. V. Chagovets, M. Rotter, D. Schmoranzer, L. Skrbek, *J. Low Temp. Phys.* **150**, 194 (2008)
- <sup>36</sup> M. Blažková, D. Schmoranzer, L. Skrbek, *Low Temp. Phys.* **34**, 298-307 (2008).
- <sup>37</sup> D. Schmoranzer, M. La Mantia, G. Sheshin, I. Gritsenko, A. Zadorozhko, M. Rotter, L. Skrbek, *J. Low Temp. Phys.* **163**, 317-344 (2011)
- <sup>38</sup> D. I. Bradley, M. Človečko, S. N. Fisher, D. Garg, E. Guise, R. P. Haley, O. Kolosov, G. R. Pickett, V. Tsepelin, D. Schmoranzer, L. Skrbek, *Phys. Rev. B* **85**, 014501 (2012).
- <sup>39</sup> D. Schmoranzer, M. Králová, V. Pilcová, W. F. Vinen and L. Skrbek, *Phys. Rev. E* **81**, 066316 (2010)
- <sup>40</sup> R. Hänninen, W. Schoepe, *J. Low Temp. Phys.* **158**, 410-414 (2010).
- <sup>41</sup> P. C. Hendry, P. V. E. McClintock, *Cryogenics* **27**, 131 (1987).
- <sup>42</sup> S. Holt, P. Skyba, *Rev. Sci. Instrum.* **83**, 064703 (2012).
- <sup>43</sup> D. I. Bradley, P. Crookston, M. J. Fear, S. N. Fisher, G. Foulds, D. Garg, A. M. Guénault, E. Guise, R. P. Haley, O. Kolosov, P. V. E. McClintock, G. R. Pickett, R. Schanen, V. Tsepelin, *J. Low Temp. Phys.* **161**, 536-547 (2010).
- <sup>44</sup> J. Guckenheimer, P. Holmes, *Nonlinear Oscillations, Dynamical Systems, and Bifurcations of Vector Fields*, Springer-Verlag, 1983.
- <sup>45</sup> E. Collin, Yu. M. Bunkov, H. Godfrin, *Phys. Rev. B* **82**, 235416 (2010).
- <sup>46</sup> F. V. Kusmartsev, *Phys. Rev. Lett.* **76**, 1880 (1996).
- <sup>47</sup> I. H. Neumann, R. J. Zieve, *Phys. Rev. B* **89**, 104521 (2014).
- <sup>48</sup> P. M. Walmsley, A. A. Levchenko, S. E. May, A. I. Golov, *J. Low Temp. Phys.* **146**, 511-523 (2007).
- <sup>49</sup> W. F. Vinen, L. Skrbek, H. A. Nichol, *J. Low Temp. Phys.* **135**, 423 (2004).
- <sup>50</sup> W. F. Vinen, L. Skrbek, *Proc. Natl. Acad. Sci. U.S.A.* **111**, 4699 (2014).
- <sup>51</sup> D. I. Bradley, R. P. Haley, S. Kafanov, M. T. Noble, G. R. Pickett, V. Tsepelin, J. Vonka, T. Wilcox, *J. Low Temp. Phys.* **186**, 1080-1091 (2016).
- <sup>52</sup> G. Ortiz, D. M. Ceperley, *Phys. Rev. Lett.* **75**, 4642-4645 (1995).
- <sup>53</sup> R. J. Donnelly, *Annu. Rev. Fluid Mech.* **25**, 325-371 (1993).
- <sup>54</sup> P. H. Roberts, J. Grant, *J. Phys. A: General Physics* **4**, 55 (1971).
- <sup>55</sup> W. F. Vinen, *Proc. Roy. Soc. Series A* **242**, 493-515 (1957).
- <sup>56</sup> P.-E. Roche, C. F. Barenghi, *Europhys. Lett.* **81**, 36002 (2008).
- <sup>57</sup> D. Duda, P. Švančara, M. La Mantia, M. Rotter, L. Skrbek, *Phys. Rev. B* **92**, 064519 (2015).
- <sup>58</sup> Statek Corporation, 512, N. Main Street, Orange, CA 92868, USA.